Journal of the National Cancer Center 5 (2025) 221–235

Contents lists available at ScienceDirect

Journal of the National Cancer Center

journal homepage: www.elsevier.com/locate/jncc

Full Length Article

The single-cell immune landscape of HIV-associated aggressive B-cell lymphoma

Xiaomei Zhang[1,†], Zailin Yang[1,†], Xiaoqing Xie[1], Jun Li[1], Qing Xiao[1], Guofa Xu[1,2], Ben Ma[3], Xudong Xie[3], Yi Liu[1], Liuyue Zhai[1], Yifeng Tang[1], Huihui Fu[1], Sanxiu He[1], Tingting Liu[1], Dehong Huang[1], Censi Zeng[1], Yixing Zhou[1], Renzhi Hu[1], Binling Guo[1], Chaoyu Wang[1], Shunsi Liang[1], Qin Luo[1], Jing Lv[1], Yingyu Nan[1], Jieping Li[1], Qiying Li[1], Shengqiang Wang[3,*], Yongzhong Wu[4,*], Yao Liu[1,*]

[1] Department of Hematology and Oncology, Chongqing University Cancer Hospital, Chongqing, China
[2] Department of Hematology and Medical Oncology, Chongqing University Fuling Hospital, Chongqing, China
[3] Department of Integrated, Chongqing University Cancer Hospital, Chongqing, China
[4] Department of Radiation Oncology, Chongqing University Cancer Hospital, Chongqing, China

ARTICLE INFO

Keywords:
HIV-associated lymphomas
Single-cell RNA sequencing
DLBCL

ABSTRACT

Background: Human immunodeficiency virus (HIV)-associated lymphomas (HAL), mainly aggressive B-cell lymphomas, pose a significant challenge in cancer research due to their multifaceted pathogenesis and aggressive clinical course. Despite the clinical importance, the genomic and immune characteristics of these lymphomas remain poorly elucidated.

Methods: We employed single-cell RNA sequencing (scRNA-seq) on lymph node samples from aggressive B-cell lymphomas, mainly including 6 cases of diffuse large B-cell lymphoma (DLBCL) and 5 cases of Burkitt lymphoma (BL) from people living with HIV (PLWH), along with 3 DLBCL cases from individuals without HIV for comparison.

Results: Malignant B cells in HAL consistently exhibited high proliferative and oxidative phosphorylation (OXPHOS)-type metabolic signatures. Moreover, these cells demonstrated loss expression of major histocompatibility complex class I (MHC-I), strategically reducing tumor immunogenicity. HAL harbors special populations of naive and atypical memory B cells that exhibited high metabolic and immune-activated transcriptional profiles. Additionally, HAL exhibited senescence-like dysfunction in T cells, characterized by the reductions in regulatory activity of Treg and cytotoxic activity of $CD8^+$ T cells, as well as decreases expression of *IL7R* genes and increases expression of *FOS* and *FOSB* genes. Our immunofluorescence results showed that the cytotoxic $CD8^+$ T cells in HAL may have a dysfunction of lytic granule polarization. Furthermore, macrophages from HAL exhibited stronger immunosuppressive transcriptional characteristics, and a robust immunosuppressive SPP1-CD44 interaction was predicted between $C1QA^+$ macrophages and T cells.

Conclusions: Our findings clearly indicate that HAL differs significantly from non-HAL, ranging from malignant B cells to the immune microenvironment. This study provides a comprehensive single-cell atlas of HIV-associated aggressive B-cell lymphomas, offering new insights into aggressiveness and immune evasion observed in HAL.

1. Introduction

Human immunodeficiency virus (HIV) infection significantly elevates the risk of lymphomas, especially aggressive B-cell lymphomas.[1] HIV-associated lymphomas (HAL) remain the most common type of cancer and a leading cause of mortality in people living with HIV (PLWH), even in the era of antiretroviral therapy (ART).[2,3] The most prevalent histological type of HAL is diffuse large B-cell lymphoma (DLBCL).[4] The pathogenesis of HAL is complex and not fully elucidated; it is primarily linked to chronic B-cell activation due to HIV-induced immune dysfunction and the loss of immune surveillance over oncogenic viruses, such as Epstein-Barr virus (EBV) and human herpesvirus 8 (HHV-8).[5,6] Our team and other research groups have reported that HAL exhibit more aggressive clinical characteristics compared to lymphomas in peo-

* Corresponding authors.
E-mail addresses: wsq38916@163.com (S. Wang), yongzhong.wu@cqu.edu.cn (Y. Wu), liuyao77@cqu.edu.cn (Y. Liu).
† These authors contributed equally to this work.

https://doi.org/10.1016/j.jncc.2025.02.001
Received 31 July 2024; Received in revised form 27 January 2025; Accepted 8 February 2025

ple without HIV (non-HAL).[7-9] These characteristics include rapid tumor growth, advanced disease stages at diagnosis, extranodal involvement, and common B symptoms. It is not fully understood what drives these differential features of HAL and the role of HIV-associated immunodeficiency in the progression of HAL. HIV primarily infects $CD4^+$ T cells, leading to their decreased numbers and impaired function. HIV also infects monocytes/macrophages, weaken their phagocytic capacity and cytokine release.[10,11] Besides, HIV infection continuously activates $CD8^+$ T cells, resulting in dysfunction such as decreased virus clearance ability and weakened proliferation capacity.[12] In tumor microenvironment, the complex interaction between tumor cells and immune cells play a crucial role in tumor immune surveillance, immune escape and immunotherapy.[13] From this, elucidating the characteristics of the tumor immune microenvironment in the context of HIV infection is helpful for understanding of HAL. In addition, HIV-encoded proteins can induce and sustain B cells activation, promote proliferation and malignant transformation of B cells.[14,15] The oncogenic effect of HIV-encoded proteins may predetermine the differences in the genetic characteristics of HAL.[16,17] However, there is no study at the single-cell level to reveal these unique lymphoma immune microenvironments and genetic properties in the context of HIV infection.

In this study, we conducted single-cell RNA sequencing (scRNA-seq) to explore the cellular landscapes of HAL, and analyzed the differences between HAL and non-HAL using DLBCL as the research focal point. This is the first study to characterize the single-cell immune landscape of HAL, offering valuable insights into their pathogenesis and potential therapeutic targets.

2. Materials and methods

2.1. Patient sample collection

We collected 17 lymph node tissues from patients admitted with lymphadenopathy through tissue aspiration or surgery. Out of these samples, 14 were obtained from PLWH. Most patients were newly diagnosed, with only one case being a relapse of DLBCL. Clinical characteristics of the participants are summarized in Supplementary Table 1.

2.2. Cell preparation for single cell RNA sequencing

Fresh tissues were dissociated using the multi-tissue dissociation kit 2 (cat#130–110–203, Miltenyi Biotec, Germany), following the manufacturer's instructions. Cell count and viability were assessed using a fluorescence cell analyzer (Countstar® Rigel S2, China) with acridine orange/propidium iodide (AO/PI) reagents. For samples with cell viability <90 %, debris and dead cells removal were carried out using the dead cell removal kit (cat#130–090–101, Miltenyi Biotec, Germany). Finally, the fresh cells were resuspended in phosphate-buffered saline (PBS) containing 0.04 % bovine serum albumin (BSA).

2.3. Single cell RNA sequencing

Single-cell RNA-Seq libraries were prepared using SeekOne® Digital Droplet System (SeekOne® DD, China) with the SeekOneDD Single Cell 3′ library preparation kit (cat#K00104–04 SeekGene, China). Briefly, the cell suspension was mixed with the reverse transcription reagent and then added to the sample well in the SeekOne® DD Chip S3. Subsequently, barcoded hydrogel beads and partitioning oil were dispensed into corresponding wells separately. After generating emulsion droplet, reverse transcription was performed at 42°C for 90 mins and then inactivated at 85°C for 5 mins. The resulting cDNA was purified and amplified by polymerase chain reaction (PCR). The amplified cDNA product was then cleaned, fragmented, end-repaired, A-tailed, and ligated to the sequencing adaptor. Indexed PCR was performed to amplify the DNA representing the 3′ polyA part of expressing genes. The indexed sequencing libraries were cleaned up with SPRI beads and quantified by quantitative PCR (cat#KK4824, KAPA Biosystems, USA). Subsequently, the libraries were sequenced on Illumina NovaSeq 6000 (Illumina, USA) with PE150 read length.

2.4. Processing the scRNA-seq data

Fastp (v0.20. 1) was utilized to trim primer sequences and remove low quality bases from the raw reads.[18] Subsequently, the cleaned reads were processed using SeekSoul Tools to generate the transcript expression matrix for further analysis. Seurat (v4.1.2) was employed to process the transcript expression matrix.[19] Briefly, the following quality control criteria were applied to filter out low-quality and potential doublet cells: feature counts over 6000 or <500, rates of mitochondrial transcripts over 20 %, and rates of hemoglobin genes over 1 %. The raw matrix was normalized using LogNormalize and SCTransform, with the effects of mitochondrial percentage regressed out. The SCTransform normalized data was then subjected to principal component analysis for dimension reduction, and the top 30 principal components were selected for single-cell clustering. The resolution parameter for clustering granularity was set to 0.5. To visualize the clusters in a two-dimensional space, non-linear dimensional reduction techniques, t-distributed stochastic neighbor embedding (tSNE) and uniform manifold approximation and projection (UMAP), were applied. Differential expression genes (DEGs) analysis was performed using the FindMarkers or FindAllMarkers function in Seurat (v4.1.2) between cell types, employing the pseudo-bulk analysis (DESeq2-LRT) in Libra (v1.0.0)[20] between HIV^+ DLBCL and HIV^- DLBCL groups ($|avg\_log_2FC| > 0.25$, P-value < 0.05).

The cell types were determined based on the expressions of known markers: MS4A1, CD19, CD79A, CD79B for B and malignant cells; IGKC for plasma cells; CD3D, CD3E, CD3G for T cells; LYZ, CD68, FCGR3A, CD14 for macrophages; LILRA4, IL3RA, JCHAIN for plasmacytoid dendritic cells (pDCs); CPA3, TPSAB1, TPSB2 for mast cells; LUM, DCN, COL3A1 for non-endothelial stromal cells; VWF, PECAM1, and CDH5 for endothelial cells; and EPCAM, KRT19, and KRT18 for epithelial cancer cells. No plasmablastic lymphoma cells (CD38 and SDC1) were identified in this plasmoblastic lymphoma (PBL) sample. For the sub-clustering of B & malignant cells, the same approach as described above was followed. Additionally, Harmony was used to remove potential batch effect between samples during sub-clustering of T cells, macrophages, and B cells. For each main cell type's sub-clustering, sub-clusters that did not express the marker genes of that particular cell type or expressed marker genes of other cell types were excluded from further analysis.

2.5. Identification of malignant B cells using infer CNVs

The InferCNV R package (v1.2.2) was utilized to estimate the initial copy number variations (CNVs) for each region.[21] The CNV of the total "B & malignant cells" sub-clusters was calculated based on the expression levels from single-cell sequencing data for each cell, using the parameters –cutoff 0.1 and –noise_filter 0.2. The reference group for CNV calculation was the "B cells" cluster, as all non-malignant B cells identified from single-sample inferCNV analysis of non-lymphomas cases (including HIV^+ RLH and HIV^+ TM_LN) were clustered within this group. The CNV score for each cell was then computed following the method described previously.[22] Briefly, the gene expression values of cells were re-standardized and limited to a range of −1 to 1. The CNV score of each cell was calculated as the quadratic sum of CNVregion.

2.6. GO and KEGG enrichment analysis

Gene Ontology (GO) and Kyoto Encyclopedia of Genes and Genomes (KEGG) enrichment analysis were performed using the ClusterProfiler R package.[23] For the sub-clusters of B & malignant cells, DEGs with a P-value adjusted (p_val_adj) <0.05 and an avg_log_2FC greater than 0.5 (indicating high expression) or less than −0.8 (indicating low expression)

were considered for the enrichment analysis. Enrichment analysis items with a corrected *P*-value (p.adjust), calculated using the Benjamini-Hochberg method, <0.05 were considered significantly enriched and were ranked according to their p.adjust values.

2.7. Gene set variation analysis

Using the Molecular Signatures Database (MSigDB), gene set variation analysis (GSVA)[24] was employed to identify differentially activated biological processes in T cells sub-clusters across different samples. The results were visualized using the pheatmap R package.

2.8. Gene set score

The gene set score for various biological processes were calculated using the AddModuleScore function in Seurat. Signature gene lists for scores were provided in Supplementary Table 10. Additionally, pathway scores were determined using gene lists obtained from validated KEGG pathways and GO biological processes.

2.9. Transcription factor regulon analysis

Transcription factor regulon analysis was performed using SCENIC (R package v0.1.7) (https://github.com/aertslab/SCENIC).[25] The expression matrices of B & malignant cells from Seurat were used to generate the regulon activity score of transcription factors for each cell type, respectively. During the analysis, genes were filtered, retaining only those with a sum of count greater than 6 % of the number of cells and detected in at least 1 % of the cells. For inferring potential transcription factor targets, the GENIE3 algorithm was chosen.

2.10. Trajectory analysis of B cells

The single-cell trajectory of B cells was analyzed by the Monocle2. Highly variable genes identified by Monocle were used to sort cells into pseudotime order. Dimensional reduction and cell ordering were performed using the DDRTree method and orderCells function. DEGs along the pseudotime were identified by differentialGeneTest function. To analyze branched-dependent genes and capture divergent developmental paths, branched expression analysis modeling (BEAM) method was applied. These branched-dependent genes were visualized using the plot_genes_branched_heatmap function. The GO biological processes enrichment analysis of these branched-dependent genes was performed using ClusterProfiler R package.

2.11. Cell–cell communication analysis

The CellChat R package (https://github.com/sqjin/CellChat) was used to infer, visualize and perform comparison analysis of intercellular communications between HIV^+ DLBCL and HIV^- DLBCL samples.[26] The total number of interactions and interaction strength, as well as the number of interactions and interaction strength among different cell types, were compared. Then, the conserved and context-specific signaling pathways were identified by comparing the information flow for each signaling pathway and the overall signaling associated with each cell type. Lastly, the up-regulated and down-regulated signaling ligand-receptor pairs from malignant cells to T cells sub-types and from C1QA macrophages to T cells sub-types were identified.

2.12. Immunofluorescence

Paraffin-embedded sections of tumor tissues (5 HIV^+ DLBCL and 5 HIV^- DLBCL) were deparaffinized in xylene followed by rehydration in ethanol. After antigen retrieval and blocking, the sections were incubated with the primary antibodies to GZMB (Abcam, ab283315, 1: 500, USA) and CD8 (Absin, abs171445, 1:200, China), MHC-I (Santa cruz, sc-55582, 1:100, USA) and CD19 (Proteintech, 27949–1-AP, 1:200, China) overnight at 4 ˚C. Then, the sections were incubated with fluorescence-conjugated secondary antibodies (ab150073 and ab175700, 1:500, Abcam, USA). Nuclei were labeled with DAPI (C1002, Beyotime, China). Images were acquired with a Leica TCS SP8 confocal microscope (Germany). LAS X office soft was used to analyze the fluorescence intensity of GZMB in cells with CD8-positive staining, and 3–5 fields were selected for each section.

2.13. Statistical analysis

DEG analysis in this study was performed by using the Wilcoxon rank-sum test or Likelihood ratio test. In Fig. 4E and 4F, statistical analyses were conducted with the GraphPad Prism 9 software, using Mann-Whitney test (nonparametric data) and two-sample *t*-test (parametric data), respectively.

3. Results

3.1. The identification of main cell types in HAL

scRNA-seq was performed on lymph node biopsy samples from 14 patients with HIV, who sought medical attention at our center from June to October 2022 due to lymphadenopathy. The clinicopathological diagnosis revealed 6 cases of DLBCL, 5 cases of burkitt lymphoma (BL), 1 case of plasmoblastic lymphoma (PBL), 1 case of reactive lymphoid hyperplasia (RLH), and a tumor metastatic lymph node (TM_LN) of nasopharyngeal carcinoma. Additionally, 3 biopsies from DLBCL patients without HIV were subjected to scRNA-seq as non-HAL controls (Fig. 1A and Supplementary Table 1). After quality control of the scRNA-seq data, 83,962 single cells were obtained for analysis. Based on canonical markers, we identified nine main cell types, including B & malignant cells (including non-malignant and malignant B cells), plasma cells, T cells, macrophages, pDCs, mast cells, non-endothelial stromal cells, endothelial cells, and epithelial cancer cells (only in the TM_LN sample) (Fig. 1B–E). Our scRNA-seq data showed no plasmablastic lymphoma cells (CD38 and SDC1) in this PBL sample, of which T cells accounted for 91 %. This might be attributed to procedural factors during the biopsy. On average, each sample contained 4939 (1047–8905) cells (Fig. 1F and Supplementary Table 2). T cells were the most dominant immune cells across all samples, followed by macrophages (Fig. 1G). The proportion of each cell type exhibited significant fluctuations across different samples, irrespective of HAL or non-HAL (Fig. 1H). Notably, there were no discernible differences in the proportions of B cells, malignant cells, plasma cells, T cells, macrophages, pDCs, mast cells, non-endothelial stromal cells, and endothelial cells between HIV^+ DLBCL and HIV^+ BL, as well as between HIV^+ DLBCL and HIV^- DLBCL (Fig. 1H–I). Above all, we revealed that the major cell type composition of HAL was similar to that of non-HAL.

3.2. The distinct characteristic of malignant B cells from HAL

To characterize malignant B cells in HAL, we first sub-clustered B & malignant cells population, and distinguished the malignant B cells from the non-malignant B cells using inferCNVs analysis (Supplementary Fig. 1A-B). From this sub-clustering, we identified a total of 11 cell clusters. Further CNV analysis revealed that 10 of these clusters were malignant B cell clusters (M01-M10) with high CNV scores, while the remaining cluster was a non-malignant B cell cluster with low CNV scores (Fig. 2A and B). The cluster of non-malignant B cells comprised 3096 cells from the majority of samples, representing 10 % of the population of B & malignant cells (Figs. 2C and D, Supplementary Fig. 1C and D). Each sub-cluster of malignant B cells predominantly contained cells from a single sample, except for cluster M04. Specifically, cluster M04 mainly

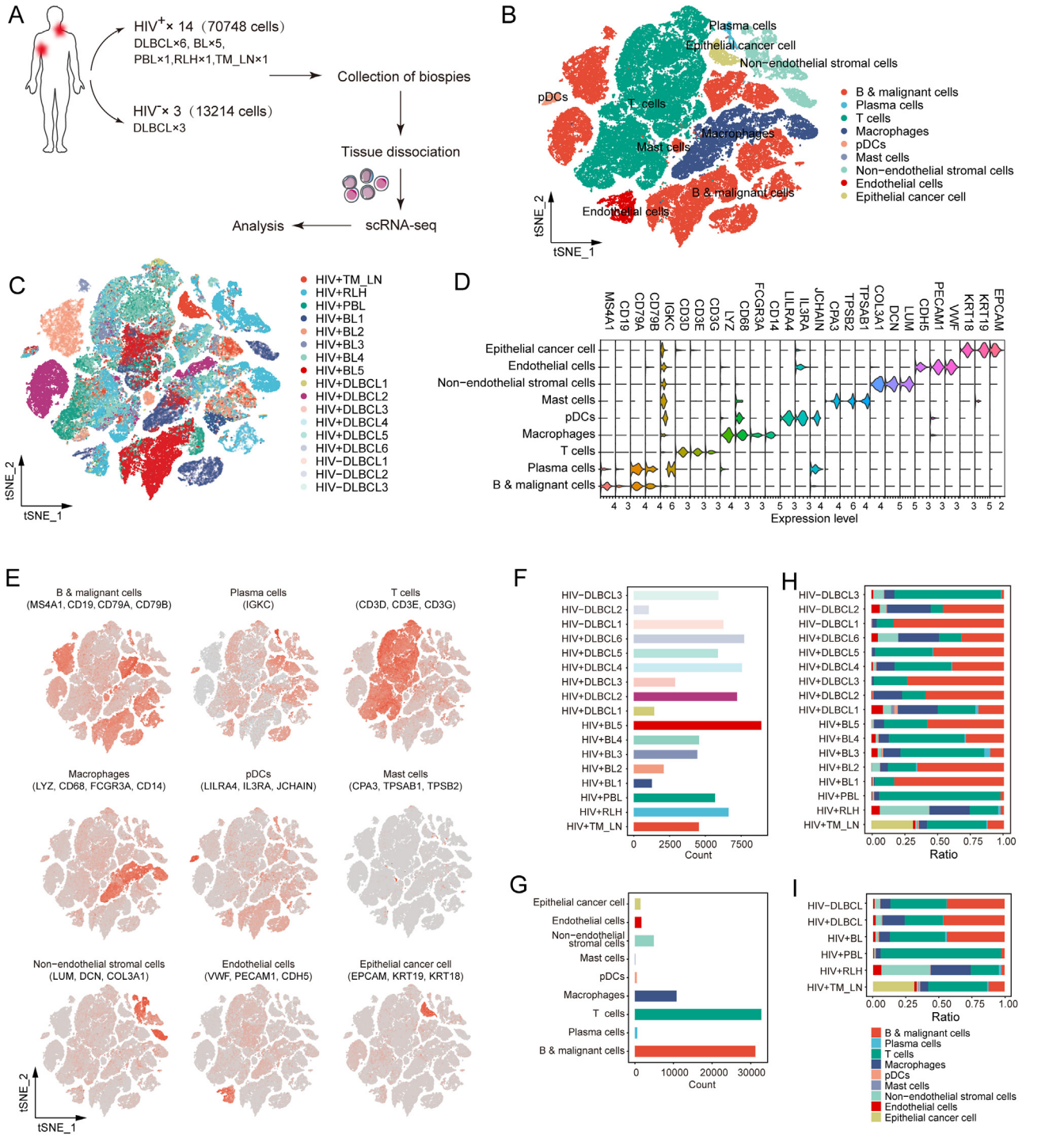

Fig. 1. Identification of main cell types in HAL using scRNA-seq data. (A) Overview of the samples collection and sequencing strategy. (B and C) The tSNE showing the distribution of total cells (83,962 cells) collected from 17 samples, colored by main cell types (B) and samples (C). (D) The violin plot showed the expression of canonical markers of main cell types. (E) tSNE showing the expression of canonical markers of main cell types. (F) The cell number of each sample. (G) The cell number of each main cell type. (H) The percentages of cell types in each sample. (I) The percentages of cell types in each disease. BL, Burkitt lymphomas; DLBCL, diffuse large B-cell lymphoma; HIV, human immunodeficiency virus; PBL, plasmoblastic lymphoma; pDC, plasmacytoid dendritic cells; RLH, reactive lymphoid hyperplasia; scRNA-seq, single-cell RNA sequencing; TM_LN, tumor metastatic lymph node; tSNE, t-distributed stochastic neighbor embedding.

consisted of malignant cells from HIV$^+$ BL2/3/4, with a minor presence of cells from HIV$^+$ DLBCL1/3/4 and HIV$^-$ DLBCL3 (Fig. 2C and D, Supplementary Fig. 1C and D). These distinctive clusters revealed both intertumoral and intratumoral heterogeneity, alongside a certain degree of intertumoral homogeneity. On the whole, M01-M02, M03-M05 and M06-M10 correspond to malignant cells originating from HIV$^-$ DLBCL, HIV$^+$ BL and HIV$^+$ DLBCL, respectively.

We performed an analysis of DEGs across the 11 sub-clusters, as shown in Supplementary Table 3. As illustrated in Supplementary Fig. 1E, each sub-cluster exhibited a unique set of highly expressed genes

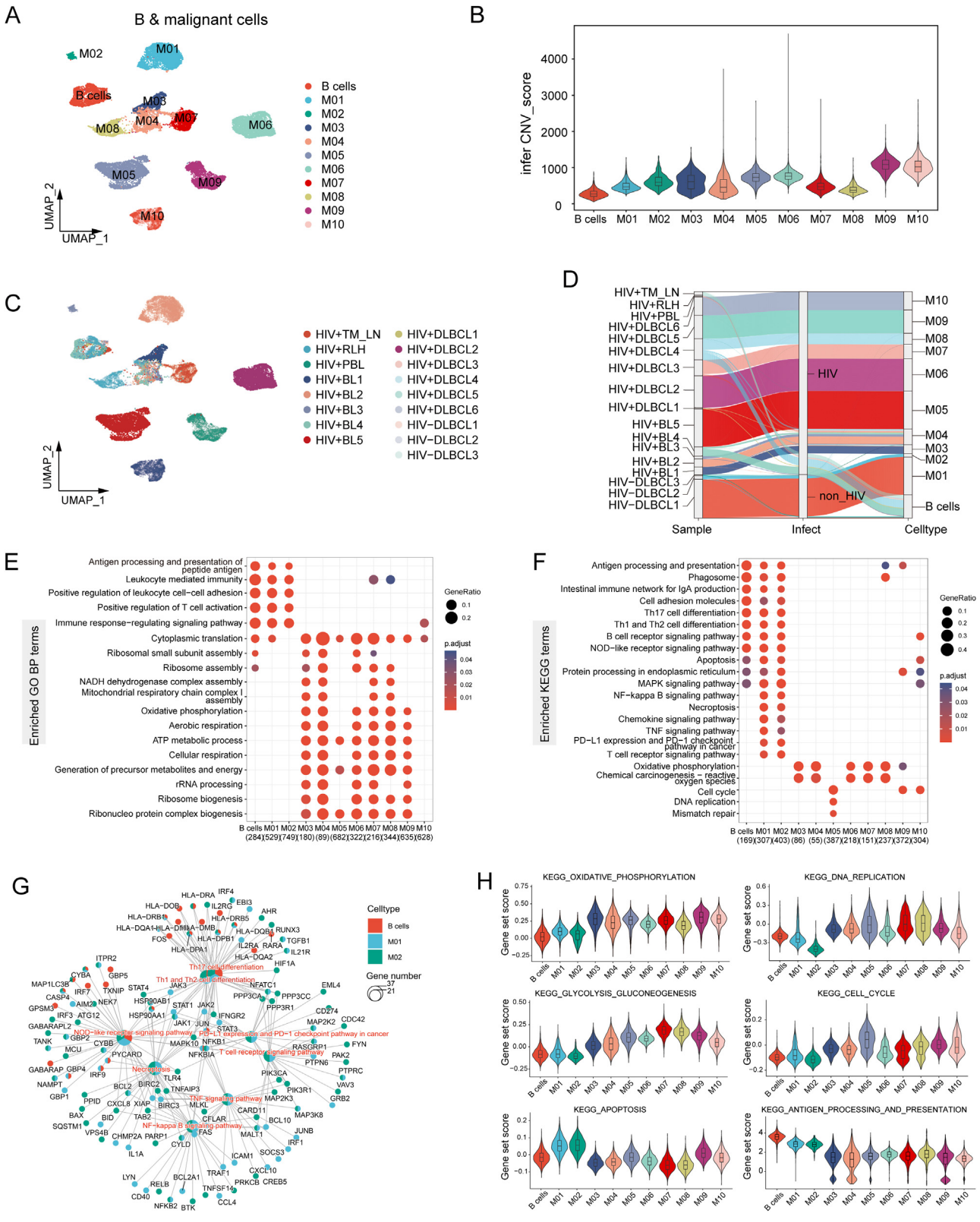

Fig. 2. Gene expression signatures of malignant B cells in HIV-associated lymphomas. (A) The UMAP showing sub-clustering of B & malignant cells, colored by cell subsets. (B) CNV scores of malignant B cell and non-malignant B cell sub-clusters. (C) UMAP showing sub-clustering of B & malignant cells, colored by samples. (D) Sankey map showing the fraction of sub-cluster and patient origin in B & malignant cells. (E and F) Dot plots showing GO biological process (E) and KEGG pathway (F) enrichment analysis of high expression genes in B & malignant cell sub-cluster. (G) Cnetplot showing the connections between genes and key KEGG pathways enriched in malignant B cells from patients without HIV. (H) Violin box plots showing gene expression scores of KEGG pathways. BL, Burkitt lymphomas; CNV, copy number variations; DLBCL, diffuse large B-cell lymphoma; HIV, human immunodeficiency virus; PBL, plasmoblastic lymphoma; RLH, reactive lymphoid hyperplasia; TM_LN, tumor metastatic lymph node; UMAP, uniform manifold approximation and projection.

(avg_log2FC > 1.5). Of the 35 key genes associated with DLBCL,[27] 23 were prominently expressed across various sub-clusters, with 15 in the HIV$^-$ DLBCL (M01-M02) and 8 in the HIV$^+$ DLBCL (M06-M10). These findings underscore the intertumoral heterogeneity and highlight the genetic disparities between HAL and non-HAL.

To further delineate the characteristics of each sub-cluster, we conducted GO and KEGG analysis of the DEGs, and identified three distinct patterns of biological activity. The first pattern, observed in B cells and the M01-M02 clusters, featured an enrichment of genes highly expressed in processes such as antigen processing and presentation, leukocyte adhesion, B cell receptor signaling, and apoptosis (Fig. 2E–F). Conversely, genes with low expression were predominantly involved in metabolic processes, including ATP metabolism and glycolysis (Supplementary Fig. 2A-B). The second pattern, exclusive to the malignant M01-M02 clusters associated with HIV$^-$ DLBCL, showed high expression of genes involved in NF-κB signaling, necroptosis, and the PD-1 checkpoint pathway in cancer, with NFKB1, JUN, and STAT3 identified as central hub genes (Fig. 1G). The third pattern, found in the malignant M03-M10 clusters from HIV$^+$ DLBCL and HIV$^+$ BL, was characterized by high expression of genes related to oxidative phosphorylation (OXPHOS), ATP metabolism, aerobic respiration, and ribosome biogenesis (Fig. 2E–F). Furthermore, genes with low expression were associated with antigen processing and presentation, as well as leukocyte adhesion (Supplementary Fig. 2A-B). Gene set score analysis further showed that malignant B cells from HAL exhibited increased activity in OXPHOS, glycolysis/gluconeogenesis, DNA replication, and the cell cycle. Conversely, these cells showed decreased activity in antigen processing and presentation and apoptosis compared to malignant B cells from non-HAL (Fig. 2H). Consistent with prior bulk-RNA sequencing studies, 16 genes involved in cell cycle progression (CCNA2, CCNB1, CDC25A) and DNA replication (MCM2, MCM4, MCM7) were significantly upregulated in malignant B cells from HAL (M03-M10). In contrast, apoptosis-related genes (BCL2, BAX, BID) were downregulated in comparison to those from non-HAL (M01-M02) (Supplementary Fig. 2C-D). These results provide critical insights into HAL, highlighting the differences in tumor biology and potential therapeutic strategies between HAL and non-HAL.

We subsequently applied SCENIC analysis to identify transcription factor regulons specific to sub-clusters. Notably, malignant B cells (M01-M02) from HIV$^-$ DLBCL displayed an activated regulon group consisting of the NFκB (REL, RELB, NFKB1, NFKB2) and AP-1 (JUND, JUN, JUNB) families (Supplementary Fig. 2E). These regulons play a role in promoting cell proliferation and survival, thereby contributing to lymphoma growth and progression. In contrast, malignant B cells from HIV$^+$ DLBCL and HIV$^+$ BL (M03-M10) demonstrated elevated activity of AKR1A1 and ENO1 regulons (Supplementary Fig. 2E), which are implicated in glycolysis and energy metabolism.[28,29] These findings suggest that a distinct metabolic profile may be fundamental to the unique biology of HAL.

3.3. The atypical B cells in HAL

Following the sub-clustering of non-malignant B cells, we identified four sub-types of B cells: two naive and two memory sub-types (Fig. 3A and B). Non-malignant B cells were found in eight out of the fourteen lymphoma samples, with their proportions ranging from 0 % to 79.19 % within the B & malignant cell population across samples (Fig. 3C). Of note, the B_naive2 and B_memory2 sub-types were observed exclusively in HIV$^+$ samples, absent in three HIV$^-$ DLBCL samples, while B_naive1 and B_memory1 sub-types were present in both HIV$^+$ and HIV$^-$ samples (Fig. 3D). The correlation heatmap and hierarchical clustering of gene-expression signatures revealed that B_memory2 was a distinct type separate from B_memory1 (Fig. 3E). A previous study suggested the presence of an unusual memory B cell subpopulation in PLWH, termed as atypical B cells (ABCs).[30] Gene signature scores were generated for our four B cell sub-types using the unique gene signatures of naive B cells, classical memory B cells (MBCs), activated MBCs and ABCs as reported in a previous study.[30] As expected, B_naive1 and B_naive2 had high naive-related gene signature scores (Fig. 3F). Notably, B_memory2 exhibited significantly high gene signature scores related to ABCs, and upregulated *HCK, TBX21, ZEB2, ZBTB32, SOX5, FCRL4, FCRL5, ITGXA* and *FGR* (Fig. 3G and Supplementary Table 4), which genes are frequently to mark ABCs.[31] In contrast, B_memory1 demonstrated a gene signature typical of MBCs. Subsequent analysis of pathway enrichment among DEGs between B_memory2 and B_memory1 revealed that upregulated genes in B_memory2 were primarily enriched in OXPHOS, nucieotide metabolism, carbon metabolism, cell cycle and apoplosis (Fig. 3H). Downregulated genes in B_memory2 were mainly enriched in pathways such as MAPK, IL-17, TNF, FaxO, NFκB signaling, mitophagy and apoplosis (Fig. 3I). All identified pathways were associated with the survival and proliferation of B cells.

Subsequent trajectory analysis of non-malignant B cells uncovered two branchpoints and five distinct states (Fig. 3J). The starting state was determined to be the branch dominated by B_naive1. This analysis identified two principal cell fate trajectories: from B_naive1 to B_memory1 in trajectory 1, and from B_naive1 through B_naive2 to B_memory2 in trajectory 2, the latter marking the unique cell fate path in HIV$^+$ DLBCL (Fig. 3J). Branch analysis to elucidate fate determinants revealed that gene clusters in trajectory 1 were enriched in biological processes related to protein folding, intrinsic apoptotic signaling, IκBK/NFκB signaling, and DNA damage repair, whereas those in trajectory 2 predominantly involved energy metabolism and immune response processes such as ATP metabolic process, ribosome biogenesis, aerobic respiration, OXPHOS, leukocyte-mediated immunity, B cell activation, and humoral immune response (Fig. 3K). Collectively, our results indicate that HAL harbors special populations of naive and atypical memory B cells that exhibit high metabolic and immune-activated transcriptional profiles.

3.4. The deficiency in immunosuppressive activity of Treg cells in HAL

Across all samples, we identified 15 sub-types of T cells using established canonical markers.[32] These sub-types included CD4_Naive (CD4, CCR7, SELL, TCF7), CD4_Th17 (KLRB1), CD4_Tfh (follicular helper T cells, CXCL13), CD4_Treg (FOXP3, IL2RA), CD8_Naive (CD8, CCR7, SELL, TCF7), CD8_Naive_ANXA1 (ANXA1), CD8_Tissue resident memory (CD69, FOS), CD8_Cytotoxic (NKG7, PFR1, GZMA, GZMB), T_proliferating (MKI67, TOP2A, PCNA) and natural killer cell-like T (NKT) cells (TRDC, FGFBP2, TYROBP, KLRD1) (Fig. 4A and B). We subdivided CD8_cytotoxic into six subsets according to their gene expression profiles[33-36]: CD8_Cytotoxic, CD8_Cytotoxic_GNLY (GNLY), CD8_Cytotoxic_Chemokine/IFN (IFNG, CCL4L2, CCL3, CCL4), CD8_Cytotoxic_XCL1 (XCL1, XCL2), CD8_Cytotoxic_Interferon (IFIT2, IFIT3), and CD8_Cytotoxic_Exh (LAG3) (Fig. 4A and B). Interestingly, CD8_Cytotoxic_Exh was infrequently observed across all samples (Fig. 4C). Consistent with the known effects of HIV infection, the CD4/CD8 ratio in HIV$^+$ samples was generally lower than HIV$^-$ samples across both peripheral blood and tumor tissues (Fig. 4D). Specifically, the reduction in CD4$^+$ T cells in HIV$^+$ DLBCL was predominantly due to a decrease in CD4_Treg cells (Fig. 4E–F). Comparatively, there was no significant variance in the proportions of CD8$^+$ T cell sub-types between HIV$^+$ DLBCL and HIV$^-$ DLBCL (Supplementary Fig. 3A).

We then assessed the differential gene expression in Treg cells between HIV$^-$ and HIV$^+$ DLBCL group (Supplementary Table 5). The upregulated genes in Treg cells from HIV$^+$ DLBCL included *FOS, FOSB, EGR1* and *SNHG32* (Fig. 4G). *FOS, FOSB* and *EGR1*, are known to be up-regulated by HIV-1 infection to promote HIV transcription and immune activation.[37-39] *SNHG32* is a non-coding RNA gene, and its functional role in T cells remains unclear. Further analysis showed significant downregulation of genes pivotal for Treg cell generation and regulatory functions, such as SATB1, TGFB1 and LAYN in HIV$^+$ DLBCL (Fig. 4G). Additionally, TNFRSF4 and TNFRSF18, which act as brake-blocks on Treg cells, were downregulated (Fig. 4G). Gene set enrichment analysis (GSEA) revealed enrichment in pathways associated with fatty acid

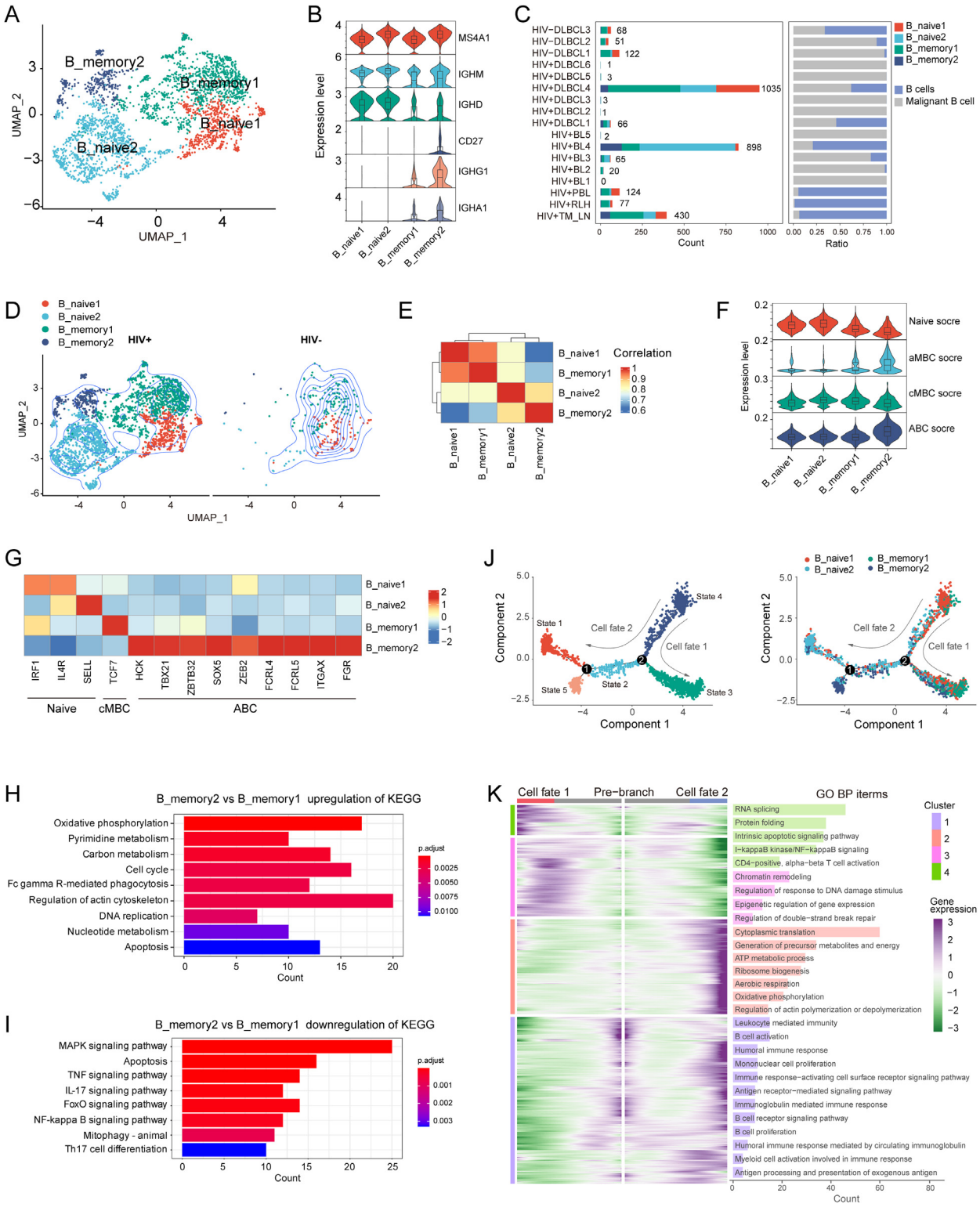

Fig. 3. Distinct non-malignant B-cell sub-types in HIV-associated lymphomas. (A) UMAP showing sub-clustering of non-malignant B cells, colored by sub-types. (B) Violin plot of markers that characterize non-malignant B cell sub-types. (C) Bar plots showing counts of non-malignant B cell sub-types in each sample and the percentage of non-malignant B cells in total B cells in each sample. (D) UMAP showing sub-clustering of non-malignant B cells from HIV^{+} and HIV^{-} samples. (E) Heatmap of Pearson correlation coefficients between the B cell sub-types. The dendrogram shows the inferred hierarchy of sub-types according to the Pearson correlation coefficients of the average expression of 1000 genes with the highest standard deviation of expression among B cell sub-types. The color scale shows the Pearson correlation coefficient. (F) Violin plot showing the gene signature scores generated for four B cell sub-types using the unique gene signatures of naive B cells, MBCs, activated MBCs and ABCs. (G) Heatmap of the average expression of marker genes in each B cell sub-types. (H and I) Bar plots showing KEGG pathway enrichment of upregulated genes (H) and downregulated genes (I) of B-memory2 compared with B-memory1 sub-types. (J) The trajectory of non-malignant B cells, colored by states and B cells sub-types. (K) Gene expression analysis of branchpoint 2. Bar plot showing GO biological process enrichment analysis of cluster genes. ABCs, atypical B cells; BL, Burkitt lymphomas; DLBCL, diffuse large B-cell lymphoma; HIV, human immunodeficiency virus; MBCs, classical memory B cells; PBL, plasmoblastic lymphoma; RLH, reactive lymphoid hyperplasia; TM_LN, tumor metastatic lymph node; UMAP, uniform manifold approximation and projection.

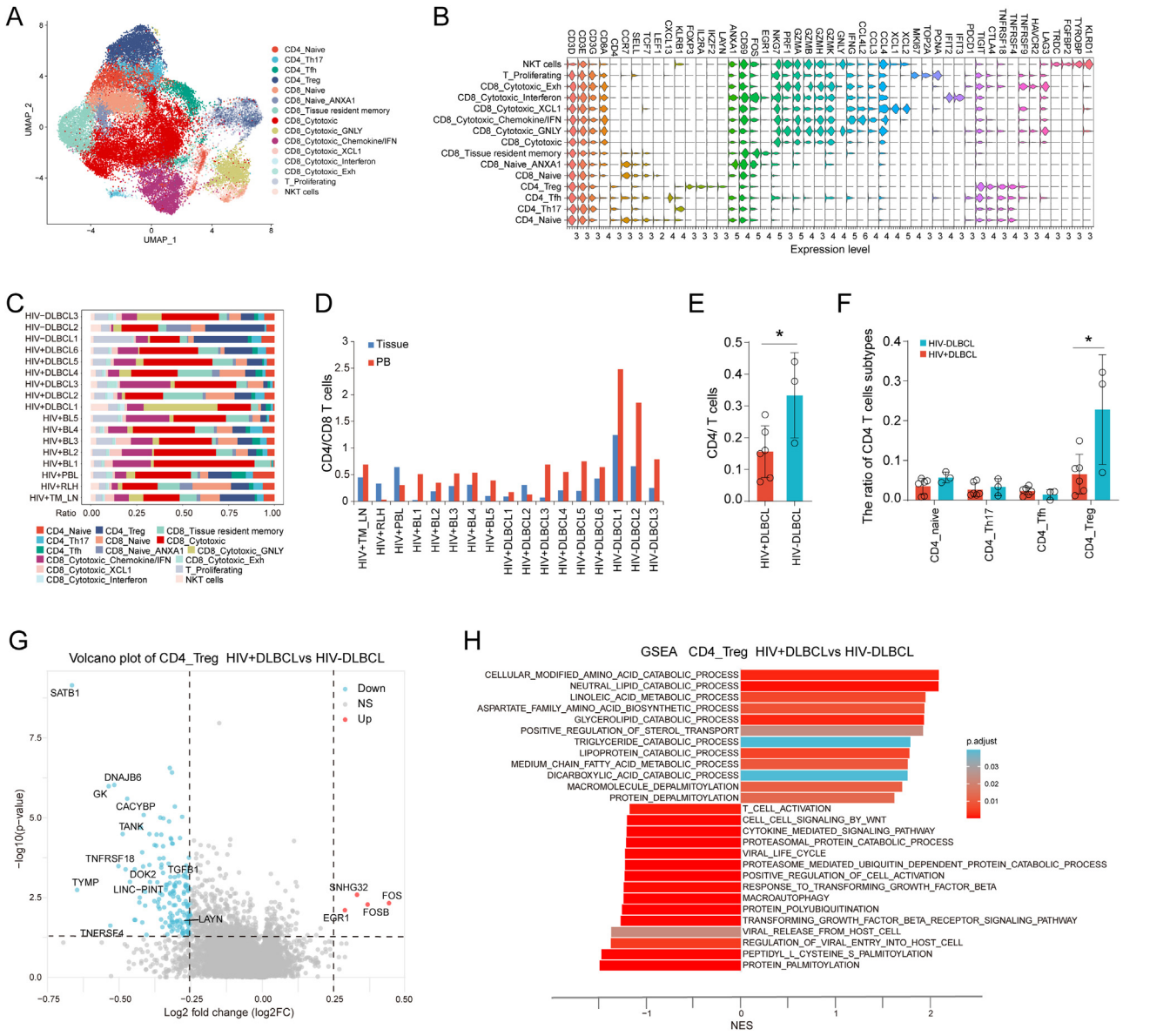

Fig. 4. Dysfunction of CD4$^+$ T cells from HIV-associated lymphomas. (A) UMAP showing sub-clustering of T cells, colored by sub-types. (B) Violin plot of markers that characterize T cell sub-types. (C) Bar plot showing the proportions of T cell sub-types in each patient. (D) Bar plot showing CD4/CD8 ratio in peripheral blood and scRNA-seq data from each sample. (E and F) The proportions of CD4$^+$ T cells (E) and sub-types (F) in T cells from HIV$^+$ and HIV$^-$ DLBCL. Values represent mean ± SD. $^*P < 0.05$ (*t*-test). (G) Volcano plot of differentially expressed genes of CD4$^+$ Treg cells between HIV$^+$ and HIV$^-$ DLBCL. (H) GSEA of GO biological process in Treg cells from HIV$^+$ DLBCL. BL, Burkitt lymphomas; DLBCL, diffuse large B-cell lymphoma; GSEA, gene set enrichment analysis; HIV, human immunodeficiency virus; NES, normalized enrichment scores; NS, not significant; PBL, plasmoblastic lymphoma; RLH, reactive lymphoid hyperplasia; Tfh, follicular helper T cell; Th, helper T cell; TM_LN, tumor metastatic lymph node; Treg, regulatory T cell; UMAP, uniform manifold approximation and projection.

catabolism and protein depalmitoylation in Treg cells from HIV$^+$ DLBCL (Fig. 4H and Supplementary Table 6). Conversely, pathways related to T cell activation, TGF-β receptor signaling pathway, viral life cycle and protein palmitoylation, were downregulated (Fig. 4H). Recent studies indicate that protein depalmitoylation significantly impairs the functions of Tregs by reducing FOXP3 protein expression.[40] Our findings indicate a potential deficiency in the immunosuppressive activity of Treg cells, extending beyond merely a decrease in their numbers in HIV$^+$ DLBCL.

3.5. *Senescence-like dysfunction of infiltrating CD8$^+$ T cells in HAL*

Similarly, the up-regulation of genes associated with T cell activation, namely *FOSB, FOS, EGR1* and *CD44*, was observed in sub-types of CD8$^+$ T cell from HIV$^+$ DLBCL compared to HIV$^-$ DLBCL (Fig. 5A and Supplementary Table 5). Conversely, *DOK2*, which encodes a negative regulator of T cell receptor signaling and is crucial for memory CD8$^+$ T cell formation and the prevention of CD8$^+$ T cell overactivation during viral infections,[41, 42] was down-regulated in sub-types of CD8$^+$ T cells from HIV$^+$ DLBCL (Fig. 5A). Moreover, CD8$^+$ memory cells from HIV$^+$ DLBCL exhibited elevated levels of the *NR4A1* genes, related to T cell unresponsiveness.[43] CD8$^+$ naive T cells from HIV$^+$ DLBCL displayed reduced expression of IL7R (Fig. 5B), correlating with T cell senescence.[44] Additionally, CD8$^+$ T cells from HIV$^+$ DLBCL exhibited significantly lower cytotoxicity scores and marginally higher exhaustion scores compared to those from HIV$^-$ DLBCL (Fig. 5C). Immunofluorescence analysis confirmed reduced GZMB protein levels in CD8$^+$ T cells from HIV$^+$ DLBCL (Fig. 5D and E). Intriguingly, HIV$^+$ DLBCL samples had a lower

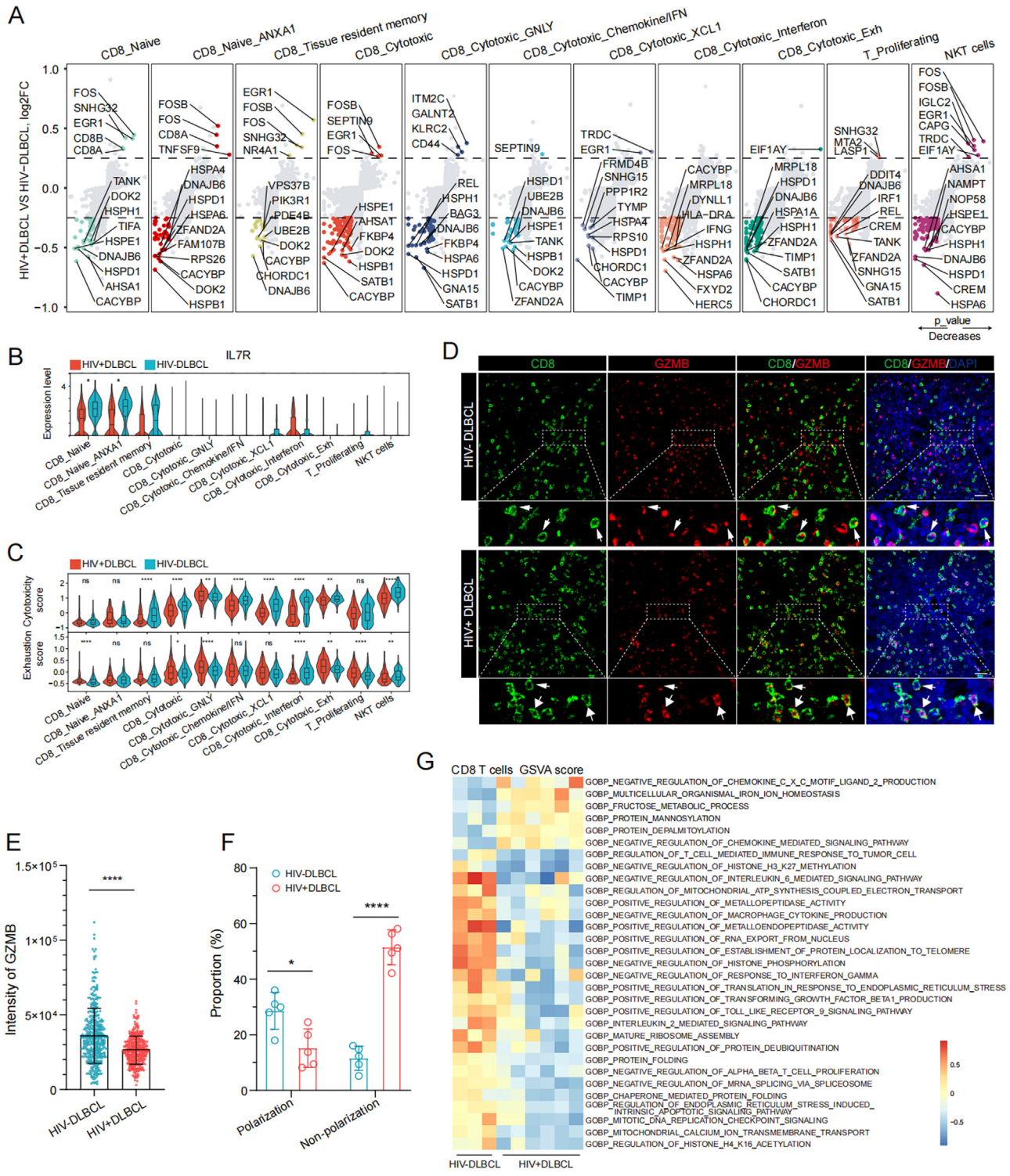

Fig. 5. Senescence-like dysfunction of CD8$^+$ T cells from HIV-associated lymphomas. (A) Volcano plot of differentially expressed genes of CD8$^+$ T cell sub-types between HIV$^+$ and HIV$^-$ DLBCL. (B) Violin box plot showing expression levels of IL7R genes in CD8$^+$ T cell sub-types. $^*P < 0.05$ (Likelihood-ratio test). (C) Exhaustion and cytotoxic score of CD8$^+$ T cell sub-types in HIV$^+$ and HIV$^-$ DLBCL. $^*P < 0.05$; $^{**}P < 0.01$; $^{****}P < 0.0001$; ns, not significant (Wilcoxon test). (D) Representative immunofluorescence images of DLBCL sections stained with antibodies against GZMB and CD8. Nuclei were stained with DAPI. Small arrows indicate GZMB polarized CD8$^+$ T cells, and large arrows indicate GZMB non-polarized CD8$^+$ T cells. Scale bar, 20 μm. (E) Immunofluorescence intensity of GZMB per CD8$^+$ T cells. Values represent mean ± SD, from 5 HIV$^-$ DLBCL samples and 5 HIV$^+$ DLBCL samples. $^{****}P < 0.0001$ (Mann-Whitney test). (F) The percentages of GZMB polarized and non-polarized CD8$^+$ T cells from HIV$^-$ DLBCL and HIV$^+$ DLBCL samples. Values represent mean ± SD, $n = 5$ samples. $^*P < 0.05$; $^{****}P < 0.0001$ (t-test). (G) Heatmap of GSVA score of CD8$^+$ T cells in HIV$^-$ DLBCL and HIV$^+$ DLBCL samples. DLBCL, diffuse large B-cell lymphoma; FC, fold change; GSVA, gene set variation analysis; HIV, human immunodeficiency virus.

proportion of CD8$^+$ T cells with polarized GZMB and a higher proportion with dispersed GZMB compared to HIV$^-$ DLBCL (Fig. 5F). This observation is consistent with the propensity of differentiated CD8$^+$ T cells from PLWH to form multifocal immune synapses rather than mature ones, thus impairing efficient cytolytic response.[45] These results indicate that, compared to non-HAL, cytotoxic CD8$^+$ T cells in HAL exhibit more pronounced functional impairments, including reduced cytotoxic capacity and an aging phenotype.

Furthermore, to determine whether this CD8$^+$ cell dysfunction in HAL is associated with HIV infection, we reanalyzed scRNA-seq data of PBMCs of six healthy individuals and six PLWH without lymphoma from previous research.[36] The PLWH cohort included three donors with high viral loads (> 100,000 RNA copies/ml of plasma) and three with low viral loads (< 20 RNA copies/ml of plasma). Consistently, we observed an increase in the expression of activation-related genes (*FOS, FOSB, EGR1* and *CD44*), along with a decrease in the expression levels of *IL7R, CD27, CD28*, and cytotoxic genes in CD4$^+$ and CD8$^+$ T cells from PLWH, irrespective of viral load (Supplementary Fig. 3B-H). These transcriptional characteristics were demonstrated a strong correlation with T cell senescence,[46-48] collectively indicating that HIV infection-driven T cell senescence could represent a significant aspect of T cells in HAL.

The top 10 down-regulated genes in CD8$^+$ T cells from HIV$^+$ DLBCL predominantly comprised genes related to protein folding, including *HSPD1, HSPB1, HSPE1, HSPH1, HSPA4, HSPA6* and *CACYBP* (Fig. 5A). GSVA further verified that the activities associated with protein folding, ribosome assembly, and T-cell-mediated immune responses to tumor cells were diminished in CD8$^+$ T cells in HIV$^+$ DLBCL (Fig. 5G and Supplementary Table 7). Additionally, biological processes pertaining to telomeres, endoplasmic reticulum stress, DNA replication, histone epigenetic modifications, mitochondrial calcium ion transport, and ATP synthesis through electron transport were found to be reduced in CD8$^+$ T cells from HIV$^+$ DLBCL (Fig. 5G). These mechanisms are intricately associated with T cell senescence, characterized by protein homeostasis imbalance, mitochondrial dysfunction, cell proliferation arrest, and epigenetic modifications.[49] Collectively, this evidence indicates a senescence-like dysfunction in CD8$^+$ T cells within HIV$^+$ DLBCL.

3.6. Infiltrating myeloid cell exacerbated immunosuppression in HAL

In our study, we identified nine sub-types of myeloid cells, which comprising four subtypes of macrophages (C1QA$^+$, S100A8$^+$, and two C1QB$^+$S100A8$^+$), three subtypes of conventional dendritic cells (cDCs) (CD1C$^+$, CLEC9A$^+$, and LAMP3$^+$), one subtype of pDCs, and one subtype of mast cells (Fig. 6A and B). No significant differences were observed in the proportions of myeloid cell subtypes between the HIV$^+$ and HIV$^-$ DLBCL (Fig. 6C). The four subtypes of macrophages exhibit distinct gene-expression profiles (Fig. 6D and Supplementary Table 8). C1QA$^+$ macrophages expressed high levels of genes (*SELENOP, APOE, FOLR2*) associated with tissue-resident macrophages (TRMs),[50] as well as *SPP1, CCL18, GPNMB* which are characteristic of M2 type tumor-associated macrophages (TAMs) with immunosuppressive and pro-tumor functions.[51,52] S100A8$^+$ macrophages showed distinct gene expression patterns, with high levels of *S100A8, S100A9, S100A12, S100A9, S100A4, FCN1, VCAN, TREM1* and *AQP9*, which are preferentially expressed in blood monocytes, indicating their likely origin from monocytes. Additionally, S100A8$^+$ macrophages exhibited elevated expression of inflammatory and chemokine genes, such as *IL1B, IL1RN, CCL3L1, CCL4, CCL4L2*, and *CXCL8*. C1QB$^+$S100A8$^+$ macrophages-1 and C1QB$^+$S100A8$^+$ macrophages-2, co-expressed genes *S100A8, S100A9, C1QA*, and *C1QB*. However, C1QB$^+$S100A8$^+$ macrophages-1 highly expressed interferon-gamma (IFN-γ) response-related genes, including *CXCL9, CXCL10, CXCL11, CCL2, CCL8, GBP1, GBP4, GBP5*, and *IDO1*, indicating potential involvement in immune response modulation.[53,54] C1QB$^+$S100A8$^+$ macrophages-2 highly expressed genes encoding metallothionein 1/2 (MT1/2), such as MT1 G, MT1H, MT1 M, MT1F, MT1X, MT1E, and MT2A. MT1/2 proteins are cysteine-rich metal-binding antioxidant proteins, previously reported to be present in some macrophages of DLBCL, but their specific role remains unknown.[55]

We then analyzed the DEGs of the main myeloid cell subtypes in HIV$^+$ DLBCL compared to HIV$^-$ DLBCL. ID2, a novel marker of M2 polarization,[56] was upregulated in main macrophage subtypes from HIV$^+$ DLBCL (Fig. 6E and Supplementary Table 9). The downregulated genes in macrophage subtypes and CD1C$^+$ cDCs primarily involved IFN-γ response-related genes and chemokines such as *CXCL8, CXCL9, CXCL10, CXCL11, IDO1, TYMP, CCL3L1*, and *CCL4L2*. Notably, myeloid cell sub-types from HIV$^+$ DLBCL consistently showed decreased expression of heat shock protein-related genes (*HSPA6, HSPE1, HSPD1, HSPH1, HSP90AA1* and *HSP90AB1*). Additionally, *HES4* are significantly downregulated in the macrophage subtypes from HIV$^+$ DLBCL. As an inhibitory transcription factor, its specific functions in macrophages remains unclear.

The functional phenotypes of macrophages have been reported to exist *in vitro* as M1 and M2 polarization states.[57] TAMs are predominantly classified as M2 type, indicative of their immunosuppressive and pro-tumor activities. Using gene set scores of M1/M2 macrophages, we discovered that macrophage in DLBCL exhibit co-expression of M1/M2 gene signatures, which varies across subtypes. C1QA$^+$ macrophages demonstrated the highest M2 signature score, as well as the phagocytosis signature score. Conversely, C1QA$^+$S100A8$^+$ macrophages-1 exhibited the highest M1 signature score (Fig. 6F and G). However, this macrophage subtype was scarcely represented across all samples (Fig. 6C). S100A8$^+$ macrophages were identified as having the highest antigen-presenting signature score. When compared to HIV$^-$ DLBCL, all macrophage subtypes in HIV$^+$ DLBCL showed elevated M2 and phagocytosis signature scores and reduced M1 and antigen-presenting signature scores (Fig. 6F and G). These results suggest that macrophages in HIV$^+$ DLBCL may contribute to a more pronounced immunosuppressive microenvironment than in HIV$^-$ DLBCL.

3.7. Crosstalk among tumor and tumor-infiltrating immune cells in HAL

To elucidate the variations in cellular communication between HIV$^+$ and HIV$^-$ lymphoma, we employed CellChat for a comparative analysis of HIV$^+$ DLBCL and HIV$^-$ DLBCL, based on gene expression profiles of receptor-ligand pairs across different cell types. It was observed that the total number of cellular interactions in HIV$^+$ DLBCL was lower than in HIV$^-$ DLBCL, albeit with no significant difference in the overall strength of these interactions (Supplementary Fig. 4A). Specifically, HIV$^+$ DLBCL demonstrated predominantly weakened interactions from malignant cells to other cells, contrasted by strengthened interactions from C1QA macrophages to other cells (Supplementary Fig. 4B). Given the pivotal role of T cells in tumor immunity, our analysis concentrated on the interactions between these cells and T cell subtypes. Notably, signaling from malignant cells to T cell subtypes crucial for T cell recruitment, adhesion, and activation—including CXCL10-CXCR3,[58] TNFSF9-TNFRSF9, IL16-CD4, LGALS9-CD44/CD45, COL93A-CD44, ALCAM-CD6, ICAM-(ITGAL+ITGB2), VCAM1-(ITGA4+ITGB1),[59] CD86/CD80-CD28, CD70-CD27 and CLEC2D/CLEC2C-KLRB1[60]—was diminished (Fig. 7A). Furthermore, interactions implicated in T cell co-inhibition, specifically LGALS9-HAVCR2 and CD86/CD80-CTLA4, were also reduced in HIV$^+$ DLBCL (Fig. 7A). Moreover, antigen-presenting signaling within the context of MHC class I/II to CD8 and CD4 T cells was lessened in HIV$^+$ DLBCL, attributed to a generalized loss of MHC- I/II gene expressions (Fig. 7A and B). This was accompanied by a more frequent loss of MHC-I protein levels in malignant cells of HIV$^+$ DLBCL (Supplementary Fig. 5). The loss of MHC-I contributes to immunogenicity reduction and immune escape of tumors.[61] The diminished interactions between malignant cells and T cell subtypes in HIV$^+$ DLBCL highlight significant impairments in T cell recruitment and activation, as well as enhanced immune evasion.

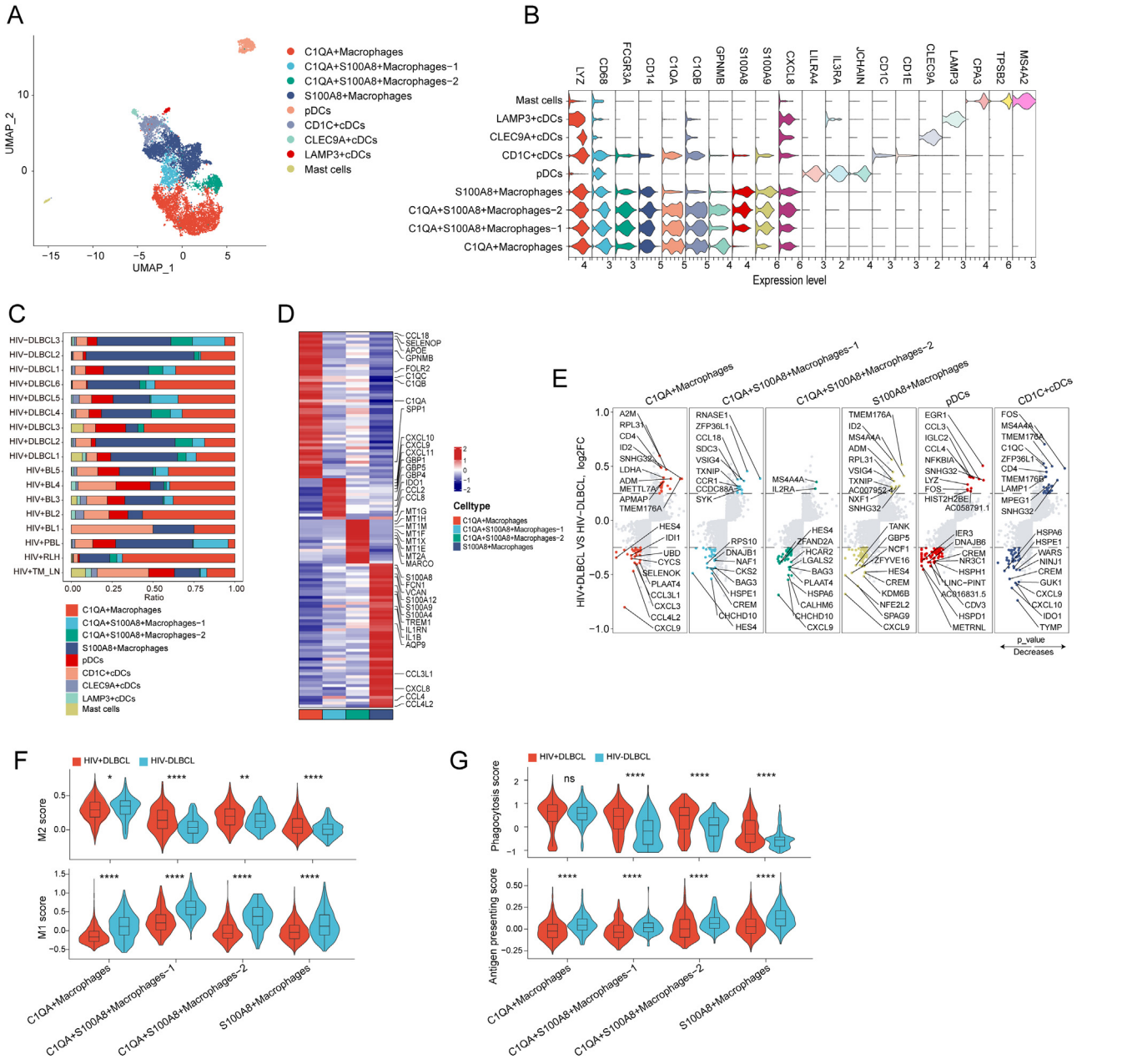

Fig. 6. Infiltrating myeloid cell exacerbated immunosuppression in HIV-associated lymphomas. (A) UMAP showing sub-clustering of myeloid cells, colored by sub-types. (B)Violin plot showing markers that characterize myeloid cell sub-types. (C) The proportions of nine sub-types of myeloid cells in each sample. (D) Heatmap of high expression genes in macrophage sub-types (avg_log$_2$FC > 1). (E) Volcano plot of differentially expressed genes of myeloid cell sub-types in HIV$^+$ DLBCL compared with HIV$^-$ DLBCL. (F) M1 and M2-type scores of macrophage sub-types from HIV$^+$ and HIV$^-$ DLBCL. (G) Antigen presenting score and phagocytosis score in macrophage sub-types from HIV$^+$ and HIV$^-$ DLBCL. $^*P < 0.05$; $^{**}P < 0.01$; $^{****}P < 0.0001$; ns, not significant (Wilcoxon test). cDC, conventional dendritic cell; DLBCL, diffuse large B-cell lymphoma; FC, fold change; HIV, human immunodeficiency virus; pDC, plasmacytoid dendritic cells; UMAP, uniform manifold approximation and projection.

Next, we analyzed the differences in interactions from C1QA$^+$ macrophages to different T cell sub-types in HIV$^+$ DLBCL compared to HIV$^-$ DLBCL. We noted a decrease in interactions facilitating T cell recruitment and activation, such as CXCL12-CXCR4, CXCL9-CXCR3, CXCL10-CXCR3, ICAM-ITGAL, ICAM-(ITGAL+ITGB2) and CD86-CD28, were reduced in HIV$^+$ DLBCL (Fig. 7C). Conversely, interactions promoting adhesion (SIGLEC1-SPN, SELPLG-SELL, LGALS9-CD44, FN1-CD44, and COL1A1-CD44) and activity inhibition (CD86-CTLA4 and SPP1-CD44) were elevated in HIV$^+$ DLBCL (Fig. 7D). Notably, SPP1-CD44 emerged as the most dominant interaction in HIV$^+$ DLBCL (Supplementary Fig. 4C), primarily originating from C1QA$^+$ macrophages, which exhibit elevated expression of SPP1 (Fig. 7E and Supplementary Fig. 4D). The SPP1-CD44 interaction is known to inhibit T cell activation and facilitate tumor immune tolerance.[62] An increased expression of CD44 in T cells, coupled with a rising trend in SPP1 in macrophages, led to a significant enhancement of the SPP1-CD44 interaction (Fig. 7F), which may intensify tumor immunosuppression in HIV$^+$ DLBCL. The analysis indicates that in HIV$^+$ DLBCL, interactions between macrophages and T cells contribute to the establishment of a more immunosuppressive microenvironment.

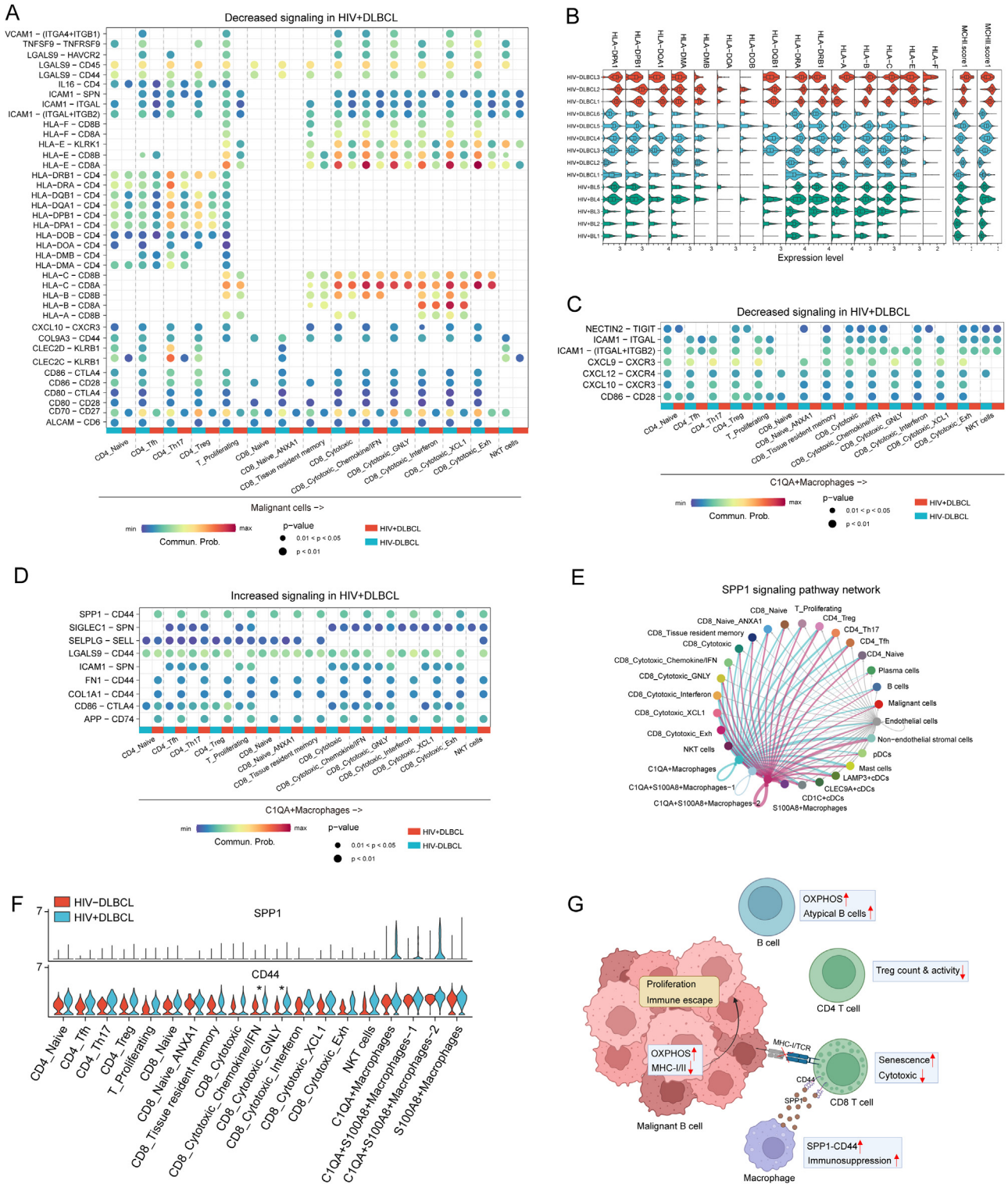

Fig. 7. Cellular crosstalk in HIV$^+$ DLBCL microenvironment. (A) The decreased signaling of interactions from malignant cells to T cell sub-types in HIV$^+$ DLBCL compared with HIV$^-$ DLBCL. (B) Violin box plot showing the expression levels of HLA family genes, and the scores of MHC-I, II family genes in each lymphoma sample. (C) The decreased signaling of interactions from C1QA$^+$ macrophages to T cell sub-types in HIV$^+$ DLBCL compared with HIV$^-$ DLBCL. (D) The increased signaling of interactions from C1QA$^+$ macrophages to T cell sub-types in HIV$^+$ DLBCL compared with HIV$^-$ DLBCL. (E) SPP1 signaling pathway network in HIV$^+$ DLBCL. (F) Violin plot showing SPP1 and CD44 expression levels in cell sub-types from HIV$^+$ DLBCL and HIV$^-$ DLBCL. $^*P < 0.05$ (Likelihood-ratio test). (G) Schematic representation of the potential mechanisms of HIV-associated lymphoma malignancy and immune escape revealed by scRNA-seq in this study. BL, Burkitt lymphomas; cDC, conventional dendritic cell; Commum Prob, communication probability; DLBCL, diffuse large B-cell lymphoma; HIV, human immunodeficiency virus; HLA, human leukocyte antigen; MHC, major histocompatibility complex; pDC, plasmacytoid dendritic cells.

4. Discussion

HIV infection significantly elevates the risk of lymphoma, with HAL exhibiting greater malignancy than conventional lymphomas though the underlying mechanisms remain unclear. This study presents a detailed single-cell atlas of HAL, showcasing a microenvironment cellular composition similar to non-HAL, except for the presence of naive and atypical memory B cell subtypes in HAL, which exhibit high metabolic and immune-activated transcriptional profiles. Distinct transcriptional expression profiles across major cell types in HAL differ from non-HAL, suggesting that HAL malignancy may stem from OXPHOS-dependent energy metabolism in malignant B cells and severe tumor immune evasion. The evasion involves the loss of antigen-presenting molecules MHC-I on malignant B cells, senescence-like dysfunction of T cell, and immunosuppressive microenvironment mediated by macrophages (Fig. 7G).

Our analysis revealed that malignant B cells in HIV$^+$ DLBCL displayed more similar transcriptional signatures with HIV$^+$ BL than with HIV$^-$ DLBCL. These signatures included high expression of genes involved in OXPHOS, and cell cycle, along with low expression of genes associated with antigen processing and presentation, apoptosis, BCR activation, and NFκB signaling. This may underscore universal traits of malignant universal features of malignant B cells from HAL. Intriguingly, all HAL cases in our study (5 BL and 6 DLBCL) might be OXPHOS-type, characterized by genes involved in mitochondrial OXPHOS metabolism, referring to consensus cluster classification (CCC) for DLBCL.[63] Within the CCC, other subtypes include BCR-DLBCL and host response (HR)-DLBCL subtypes. The cell of origin (COO) framework categorizes DLBCL into germinal center B-cell (GCB)-like, activated B-cell-like, and unclassified DLBCL. In the general population, OXPHOS-DLBCL constitutes approximately 25 % of both GCB and non-GCB DLBCL cases.[63] However, in PLWH, all six DLBCL cases (five GCB and one non-GCB) and five BL exhibited OXPHOS-like characteristics in this study. Previous research has highlighted that non-GCB DLBCL uniquely depends on BCR-dependent NFκB signaling activation, a characteristic absent in GC-derived BL and GCB DLBCL.[64] Our discovery that the case of non-GCB DLBCL from patient with HIV exhibited transcriptional signature linked to lower BCR activation and NFκB signaling. This discrepancy invites further investigation into the genetic divergences between HAL and non-HAL.

In the general population, approximately 50 % of DLBCL cases lack cell-surface expression of MHC-I. Our findings indicate that MHC-I loss may be more prevalent in HAL, leading to diminished tumor immunogenicity and subsequent evasion of cytotoxic T cell recognition. This reduction in MHC-I expression likely results from various mechanisms, including HLA-I, EZH2 mutation.[65,66] Moreover, recent research suggests that disturbances in mitochondrial electron transport can influence the transcriptional and epigenetic activation of MHC-I via succinate levels.[67] This phenomenon suggests that the observed decrease in MHC-I expression in malignant B cells from HAL could be linked to increased OXPHOS activity. However, this hypothesis requires further empirical confirmation.

T cell senescence-like dysfunction may represent a significant mechanism of immune escape in HAL. Previous studies had documented senescence in T cells of PLWH, characterized by various indicators such as low CD4/CD8 ratio, low naïve/memory cell ratio, decreased TCR diversity, reduced responsiveness to vaccines, decreased proliferative potential, expansion of CD28$^-$ effector T cells, and telomerase shortening.[68,69] In this study, T cells in HAL exhibited reduced IL7R gene expression and enhanced *FOS* and *FOSB* gene expression. Loss IL7R in T cells is as potential biomarkers for aging-associated immunodeficiency.[44] The FOS family of proteins are components of the activator protein-1 (AP-1) transcription factor complex. Several studies have pinpointed transcriptional activation of AP-1 as a prominent and conserved signature of both activation and senescence of T cell, altering chromatin opening and remodeling enhancer landscape.[46,48,70] Recently, Wei et al. identified increased AP-1 accessibility in transcriptionally active HIV-1-infected cells.[71] All of these suggest AP-1 may acts as a crucial intermediary linking T cell activation to senescence under HIV infection. Moreover, heat shock proteins, vital for protein folding, were notably reduced in T cells from HAL, potentially leading to misfolded protein buildup and ensuing mitochondrial dysfunction.[72] Mitochondrial dysfunction in T cells has been demonstrated in PLWH both on and off ART[73] and contributed to T cell senescence.[74] The senescence of T cells not only impairs their ability to combat tumors but also weakens the efficacy of tumor immunotherapy.[75,76] On the whole, senescence-like dysfunction of T cells may be a significant target for research and potential therapeutic strategies in HAL.

Macrophages are the most common infiltrating myeloid cells in HAL. Consistent with previous research,[50] C1QA$^+$ macrophages expressed high levels of genes associated with TRMs and M2 type TAMs with immunosuppressive and pro-tumor functions. SPP1 is highly expressed in C1QA$^+$ macrophages and associated with the M2 phenotype. Recent research found that macrophage polarity, defined by CXCL9:SPP1 ratio had a noticeably strong prognostic association in a variety of solid tumors.[77] In this study, CXCL9 was markedly decreased in macrophages from HAL, including these SPP1$^+$ macrophages. It appears that these SPP1$^+$ macrophages have stronger pro-tumor properties in HAL. Furthermore, cellular communication analysis showed SPP1-CD44 interaction was reinforced in HAL. CD44 is a marker of T cell activation during immune responses and aging.[78,79] The interaction between SPP1 and CD44 can directly suppress T cell activation.[62] Increased expression of CD44 in T cell subtype was observed in HAL. Therefore, SPP1$^+$ macrophages warrant further investigation in exploring immune escape mechanisms in HAL and could potentially open avenues for innovative immunotherapeutic approaches.

Our study presents a single-cell atlas of HAL. However, limitations such as the small sample size require further validation with larger cohorts. Despite this, our findings reveal significant differences between HAL and non-HAL, highlighting the need to understand HAL's unique biology. Future research should explore MHC loss mechanisms, T cell senescence-like dysfunction, and the role of immunosuppressive macrophages, as these may uncover new targets and strategies for tumor immunotherapy in PLWH.

Declaration of competing interest

The authors declare that they have no known competing financial interests or personal relationships that could have appeared to influence the work reported in this paper.

Ethics statement

This study was performed in accordance with the Declaration of Helsinki and was approved by the Chongqing University Institutional Review Board (approval number: CZLS2021069-A), and each patient provided written informed consent.

Data availability

Data supporting conclusions in this article are provided in Supplementary Tables 1–10. The raw data of scRNA-seq in this study are publicly accessible (HRA005638) at Genome Sequence Archive in National Genomics Data Center, China National Center for Bioinformation/Beijing Institute of Genomics, Chinese Academy of Sciences (https://ngdc.cncb.ac.cn/gsa-human). Previously published scRNA-seq data are available at GEO under accession number GSE157829, GSE190510, and GSE243629.

Acknowledgments

We are grateful to Prof. Zhian Hu (Department of Physiology, Army Medical University, Chongqing, China) for his advices on

study design. This study was supported by Natural Science Foundation of Chongqing, China (grant numbers: CSTB2022NSCQ-MSX1150, 2023NSCQ-MSX3235), Fundamental Research Funds for the Central Universities (grant numbers: 2022CDJYGRH-001, 2023CDJYGRH-YB02) and Chongqing Professional Talents Plan (grant number: cstc2022ycjh-bgzxm0048).

Author contributions

X. Zhang, S. Wang, Y. Wu, and Y. Liu designed this study. J. Li, Z. Yang, B. Ma, X. Xie, C. Wang performed sample preparation. X. Zhang, Z. Yang, Q Xiao, G. Xu performed single-cell RNA sequence. X. Zhang, Z. Yang, H. Fu, S. He performed bioinformatic analysis. T. Liu, D. Huang, C. Zeng, S. Liang, Y. Zhou, R. Hu, B. Guo, Q. Luo, J. Lv collated clinical information and administration. Y. Tang, L. Zhai, performed immunofluorescence staining. X. Zhang, X. Xie prepared the manuscript. Z. Yang, Y. Liu, Y. Nan, J. Li, Q. Li revised the manuscript.

Supplementary materials

Supplementary material associated with this article can be found, in the online version, at doi:10.1016/j.jncc.2025.02.001.

References

1. Chen Y, Zhao J, Sun P, et al. Estimates of the global burden of non-Hodgkin lymphoma attributable to HIV: a population attributable modeling study. *eClinicalMedicine*. 2023;67:102370.
2. Simard EP, Pfeiffer RM, Engels EA. Cumulative incidence of cancer among individuals with acquired immunodeficiency syndrome in the United States. *Cancer*. 2011;117(5):1089–1096.
3. Polesel J, Clifford GM, Rickenbach M, et al. Non-hodgkin lymphoma incidence in the Swiss HIV Cohort Study before and after highly active antiretroviral therapy. *AIDS*. 2008;22(2):301–306.
4. Meister A, Hentrich M, Wyen C, Hübel K. Malignant lymphoma in the HIV-positive patient. *Eur J Haematol*. 2018;101(1):119–126.
5. Dolcetti R, Gloghini A, Caruso A, Carbone A. A lymphomagenic role for HIV beyond immune suppression? *Blood*. 2016;127(11):1403–1409.
6. Smedby KE, Ponzoni M. The aetiology of B-cell lymphoid malignancies with a focus on chronic inflammation and infections. *J Intern Med*. 2017;282(5):360–370.
7. Wang C, Liu J, Liu Y. Progress in the treatment of HIV-associated lymphoma when combined with the antiretroviral therapies. *Front Oncol*. 2022;11:798008.
8. de Carvalho PS, Leal FE, Soares MA. Clinical and molecular properties of human immunodeficiency virus-related diffuse large B-cell lymphoma. *Front Oncol*. 2021;11:675353.
9. Wang C, Wu Y, Liu J, et al. Impact of initial chemotherapy cycles and clinical characteristics on outcomes for HIV-associated diffuse large B cell lymphoma patients: the Central and Western China AIDS Lymphoma League 001 study (CALL-001 study). *Front Immunol*. 2023;14:1153790.
10. Kedzierska K, Azzam R, Ellery P, Mak J, Jaworowski A, Crowe SM. Defective phagocytosis by human monocyte/macrophages following HIV-1 infection: underlying mechanisms and modulation by adjunctive cytokine therapy. *J Clin Virol*. 2003;26(2):247–263.
11. Galvão-Lima LJ, Espíndola MS, Soares LS, et al. Classical and alternative macrophages have impaired function during acute and chronic HIV-1 infection. *Braz J Infect Dis*. 2017;21(1):42–50.
12. Collins DR, Gaiha GD, Walker BD. CD8+ T cells in HIV control, cure and prevention. *Nat Rev Immunol*. 2020;20(8):471–482.
13. Liu Y, Zhou X, Wang X. Targeting the tumor microenvironment in B-cell lymphoma: challenges and opportunities. *J Hematol Oncol*. 2021;14(1):125.
14. Carroll VA, Lafferty MK, Marchionni L, Bryant JL, Gallo RC, Garzino-Demo A. Expression of HIV-1 matrix protein p17 and association with B-cell lymphoma in HIV-1 transgenic mice. *Proc Natl Acad Sci U S A*. 2016;113(46):13168–13173.
15. Dolcetti R, Giagulli C, He W, et al. Role of HIV-1 matrix protein p17 variants in lymphoma pathogenesis. *Proc Natl Acad Sci U S A*. 2015;112(46):14331–14336.
16. Maguire A, Chen X, Wisner L, et al. Enhanced DNA repair and genomic stability identify a novel HIV-related diffuse large B-cell lymphoma signature. *Int J Cancer*. 2019;145(11):3078–3088.
17. Capello D, Scandurra M, Poretti G, et al. Genome wide DNA-profiling of HIV-related B-cell lymphomas. *Br J Haematol*. 2010;148(2):245–255.
18. Chen S, Zhou Y, Chen Y, Gu J. fastp: an ultra-fast all-in-one FASTQ preprocessor. *Bioinformatics*. 2018;34(17):i884–i890.
19. Hao Y, Hao S, Andersen-Nissen E, et al. Integrated analysis of multimodal single-cell data. *Cell*. 2021;184(13):3573–3587.e3529.
20. Squair JW, Gautier M, Kathe C, et al. Confronting false discoveries in single-cell differential expression. *Nat Commun*. 2021;12(1):5692.
21. Patel AP, Tirosh I, Trombetta JJ, et al. Single-cell RNA-seq highlights intratumoral heterogeneity in primary glioblastoma. *Science*. 2014;344(6190):1396–1401.
22. Peng J, Sun B-F, Chen C-Y, et al. Single-cell RNA-seq highlights intra-tumoral heterogeneity and malignant progression in pancreatic ductal adenocarcinoma. *Cell Res*. 2019;29(9):725–738.
23. Yu G, Wang LG, Han Y, He QY. clusterProfiler: an R package for comparing biological themes among gene clusters. *OMICS*. 2012;16(5):284–287.
24. Hänzelmann S, Castelo R, Guinney J. GSVA: gene set variation analysis for microarray and RNA-seq data. *BMC Bioinformatics*. 2013;14(1):7.
25. Aibar S, González-Blas CB, Moerman T, et al. SCENIC: single-cell regulatory network inference and clustering. *Nat Methods*. 2017;14(11):1083–1086.
26. Jin S, Guerrero-Juarez CF, Zhang L, et al. Inference and analysis of cell-cell communication using CellChat. *Nat Commun*. 2021;12(1):1088.
27. Wright GW, Huang DW, Phelan JD, et al. A probabilistic classification tool for genetic subtypes of diffuse large B cell lymphoma with therapeutic implications. *Cancer Cell*. 2020;37(4):551–568.e514.
28. Zhou H-L, Zhang R, Anand P, et al. Metabolic reprogramming by the S-nitroso-CoA reductase system protects against kidney injury. *Nature*. 2019;565(7737):96–100.
29. Huang CK, Sun Y, Lv L, Ping Y. ENO1 and cancer. *Mol Ther Oncolytics*. 2022;24:288–298.
30. Holla P, Dizon B, Ambegaonkar AA, et al. Shared transcriptional profiles of atypical B cells suggest common drivers of expansion and function in malaria, HIV, and autoimmunity. *Sci Adv*. 2021;7(22):eabg8384.
31. Gao X, Cockburn IA. The development and function of CD11c+ atypical B cells - insights from single cell analysis. *Front Immunol*. 2022;13:979060.
32. Tirosh I, Izar B, Prakadan SM, et al. Dissecting the multicellular ecosystem of metastatic melanoma by single-cell RNA-seq. *Science*. 2016;352(6282):189–196.
33. Wang XM, Zhang JY, Xing X, et al. Global transcriptomic characterization of T cells in individuals with chronic HIV-1 infection. *Cell Discov*. 2022;8(1):29.
34. Song G, Shi Y, Zhang M, et al. Global immune characterization of HBV/HCV-related hepatocellular carcinoma identifies macrophage and T-cell subsets associated with disease progression. *Cell Discov*. 2020;6(1):90.
35. Nicolet BP, Guislain A, van Alphen FPJ, et al. CD29 identifies IFN-gamma-producing human CD8(+) T cells with an increased cytotoxic potential. *Proc Natl Acad Sci U S A.*. 2020;117(12):6686–6696.
36. Wang S, Zhang Q, Hui H, Agrawal K, Karris MAY, Rana TM. An atlas of immune cell exhaustion in HIV-infected individuals revealed by single-cell transcriptomics. *Emerg Microbes Infect*. 2020;9(1):2333–2347.
37. Wong LM, Li D, Tang Y, et al. Human immunodeficiency virus-1 latency reversal via the induction of early growth response protein 1 to bypass protein kinase C agonist-associated immune activation. *Front Microbiol*. 2022;13:836831.
38. Fan Y, Zou W, Green LA, Kim BO, He JJ. Activation of egr-1 expression in astrocytes by HIV-1 tat: new insights into astrocyte-mediated tat neurotoxicity. *J Neuroimmune Pharmacol*. 2011;6(1):121–129.
39. Varin A, Manna SK, Quivy V, et al. Exogenous nef protein activates NF-kB, AP-1, and c-jun N-terminal kinase and stimulates HIV transcription in promonocytic cells: role in AIDS pathogenesis. *J Biol Chem*. 2003;278(4):2219–2227.
40. Zhou B, Zhang M, Ma H, et al. Distinct palmitoylation of Foxp3 regulates the function of regulatory T cells via palmitoyltransferases. *Cell Mol Immunol*. 2024;21(7):787–789.
41. Yasuda T, Bundo K, Hino A, et al. Dok-1 and Dok-2 are negative regulators of T cell receptor signaling. *Int Immunol*. 2007;19(4):487–495.
42. Laroche-Lefebvre C, Yousefi M, Daudelin J-F, et al. Dok-1 and Dok-2 regulate the formation of memory CD8+ T cells. *J Immunol (Baltimore, Md : 1950)*. 2016;197(9):3618–3627.
43. Liu X, Wang Y, Lu H, et al. Genome-wide analysis identifies NR4A1 as a key mediator of T cell dysfunction. *Nature*. 2019;567(7749):525–529.
44. Ucar D, Marquez EJ, Chung CH, et al. The chromatin accessibility signature of human immune aging stems from CD8(+) T cells. *J Exp Med*. 2017;214(10):3123–3144.
45. Anikeeva N, Steblyanko M, Kuri-Cervantes L, Buggert M, Betts MR, Sykulev Y. The immune synapses reveal aberrant functions of CD8 T cells during chronic HIV infection. *Nat Commun*. 2022;13(1):6436.
46. Martínez-Zamudio RI, Roux P-F, de Freitas JANLF, et al. AP-1 imprints a reversible transcriptional programme of senescent cells. *Nat Cell Biol*. 2020;22(7):842–855.
47. Delpoux A, Marcel N, Michelini RH, et al. FOXO1 constrains activation and regulates senescence in CD8 T cells. *Cell Rep*. 2021;34(4):108674.
48. Karakaslar EO, Katiyar N, Hasham M, et al. Transcriptional activation of Jun and Fos members of the AP-1 complex is a conserved signature of immune aging that contributes to inflammaging. *Aging cell.*. 2023;22(4):e13792.
49. Mittelbrunn M, Kroemer G. Hallmarks of T cell aging. *Nat. Immunol.*. 2021;22(6):687–698.
50. Domanska D, Majid U, Karlsen VT, et al. Single-cell transcriptomic analysis of human colonic macrophages reveals niche-specific subsets. *J. Exp. Med.*. 2022;219(3):e20211846.
51. Cardoso AP, Pinto ML, Castro F, et al. The immunosuppressive and pro-tumor functions of CCL18 at the tumor microenvironment. *Cytokine Growth Factor Rev*. 2021;60:107–119.
52. Zhang H, Zhang S, Dang X, Lin L, Ren L, Song R. GPNMB plays an active role in the M1/M2 balance. *Tissue and Cell.*. 2022;74:101683.
53. Furudate S, Fujimura T, Kakizaki A, Hidaka T, Asano M, Aiba S. Tumor-associated M2 macrophages in mycosis fungoides acquire immunomodulatory function by interferon alpha and interferon gamma. *J Dermatol Sci*. 2016;83(3):182–189.
54. Workman MJ, Troisi E, Targan SR, Svendsen CN, Barrett RJ. Modeling intestinal epithelial response to interferon-γ in induced pluripotent stem cell-derived Human intestinal organoids. *Int J Mol Sci*. 2021;22(1):288.
55. Poulsen CB, Borup R, Borregaard N, Nielsen FC, Møller MB, Ralfkiaer E. Prognostic significance of metallothionein in B-cell lymphomas. *Blood*. 2006;108(10):3514–3519.

56. Saliba AE, Li L, Westermann AJ, et al. Single-cell RNA-seq ties macrophage polarization to growth rate of intracellular Salmonella. *Nat Microbiol*. 2016;2(2):16206.
57. Gordon S. Alternative activation of macrophages. *Nat Rev Immunol*. 2003;3(1):23–35.
58. Mikucki ME, Fisher DT, Matsuzaki J, et al. Non-redundant requirement for CXCR3 signalling during tumoricidal T-cell trafficking across tumour vascular checkpoints. *Nat Commun*. 2015;6(1):7458.
59. Van Seventer GA, Shimizu Y, Horgan KJ, Shaw S. The LFA-1 ligand ICAM-1 provides an important costimulatory signal for T cell receptor-mediated activation of resting T cells. *J Immunol*. 1990;144(12):4579–4586.
60. Fergusson Joannah R, Smith Kira E, Fleming Vicki M, et al. CD161 defines a transcriptional and functional phenotype across distinct human T cell lineages. *Cell Rep*. 2014;9(3):1075–1088.
61. Jhunjhunwala S, Hammer C, Delamarre L. Antigen presentation in cancer: insights into tumour immunogenicity and immune evasion. *Nat Rev Cancer*. 2021;21(5):298–312.
62. Klement JD, Paschall AV, Redd PS, et al. An osteopontin/CD44 immune checkpoint controls CD8+ T cell activation and tumor immune evasion. *J Clin Invest*. 2018;128(12):5549–5560.
63. Monti S, Savage KJ, Kutok JL, et al. Molecular profiling of diffuse large B-cell lymphoma identifies robust subtypes including one characterized by host inflammatory response. *Blood*. 2005;105(5):1851–1861.
64. Phelan JD, Young RM, Webster DE, et al. A multiprotein supercomplex controlling oncogenic signalling in lymphoma. *Nature*. 2018;560(7718):387–391.
65. Fangazio M, Ladewig E, Gomez K, et al. Genetic mechanisms of HLA-I loss and immune escape in diffuse large B cell lymphoma. *Proc Natl Acad Sci U S A*.. 2021;118(22):e2104504118.
66. Ennishi D, Takata K, Béguelin W, et al. Molecular and genetic characterization of MHC deficiency identifies EZH2 as therapeutic target for enhancing immune recognition. *Cancer Discov*. 2019;9(4):546–563.
67. Mangalhara KC, Varanasi SK, Johnson MA, et al. Manipulating mitochondrial electron flow enhances tumor immunogenicity. *Science*. 2023;381(6664):1316–1323.
68. Kalayjian RC, Landay A, Pollard RB, et al. Age-related immune dysfunction in health and in human immunodeficiency virus (HIV) disease: association of age and HIV infection with naive CD8+ cell depletion, reduced expression of CD28 on CD8+ cells, and reduced thymic volumes. *J Infect Dis*. 2003;187(12):1924–1933.
69. Desai S, Landay A. Early immune senescence in HIV disease. *Curr HIV/AIDS Rep*. 2010;7(1):4–10.
70. Yukawa M, Jagannathan S, Vallabh S, et al. AP-1 activity induced by co-stimulation is required for chromatin opening during T cell activation. *J Exp Med*. 2019;217(1):e20182009.
71. Wei Y, Davenport TC, Collora JA, et al. Single-cell epigenetic, transcriptional, and protein profiling of latent and active HIV-1 reservoir revealed that IKZF3 promotes HIV-1 persistence. *Immunity*. 2023;56(11):2584–2601.e2587.
72. Shin C-S, Meng S, Garbis SD, et al. LONP1 and mtHSP70 cooperate to promote mitochondrial protein folding. *Nat Commun*. 2021;12(1):265.
73. Korencak M, Byrne M, Richter E, et al. Effect of HIV infection and antiretroviral therapy on immune cellular functions. *JCI insight*. 2019;4(12):e126675.
74. Desdín-Micó G, Soto-Heredero G, Aranda JF, et al. T cells with dysfunctional mitochondria induce multimorbidity and premature senescence. *Science*. 2020;368(6497):1371–1376.
75. Ferrara R, Naigeon M, Auclin E, et al. Circulating T-cell immunosenescence in patients with advanced non–small cell lung cancer treated with single-agent PD-1/PD-L1 inhibitors or platinum-based chemotherapy. *Clin Cancer Res*. 2021;27(2):492–503.
76. Liu X, Hartman CL, Li L, et al. Reprogramming lipid metabolism prevents effector T cell senescence and enhances tumor immunotherapy. *Sci Transl Med*. 2021;13(587):eaaz6314.
77. Bill R, Wirapati P, Messemaker M, et al. CXCL9:SPP1 macrophage polarity identifies a network of cellular programs that control human cancers. *Science*. 2023;381(6657):515–524.
78. Baaten BJG, Li C-R, Bradley LM. Multifaceted regulation of T cells by CD44. *Commun Integr Biol*. 2010;3(6):508–512.
79. Soto-Heredero G, MMGdl Heras, Escrig-Larena JI, Mittelbrunn M. Extremely differentiated T cell subsets contribute to tissue deterioration during aging. *Annu Rev Immunol*. 2023;41(1):181–205.